Distribution and failure modes of the landslides in Heitai terrace, China

Dalei Peng[a], Qiang Xu[a,*], Fangzhou Liu[b], Yusen He[c], Shuai Zhang[d], Xing Qi[a], Kuanyao Zhao[a], Xianlin Zhang[a]

[a] State Key Laboratory of Geohazard Prevention and Geoenvironment Protection, Chengdu University of Technology, Chengdu, Sichuan 610059, China
[b] School of Civil and Environmental Engineering, Georgia Institute of Technology, Atlanta, GA, USA
[c] Intelligent Systems Laboratory, 2139 Seamans Center, Mechanical and Industrial Engineering, University of Iowa, Iowa City, IA 52242-1527, USA
[d] MOE Key Laboratory of Soft Soils and Geoenvironmental Engineering, Zhejiang University, Zheda Road #38, Hangzhou 310027, China

ARTICLE INFO

ABSTRACT

Agricultural irrigation has increased the groundwater level in the Heitai terrace (part of the Heifangtai terrace) by 20 m over nearly five decades, which causes 3–5 landslides each year at the edge of the terrace. The Heitai terrace is of great interest in the study of loess-related landslides; but there is no unanimous agreement on the types of either the landslides in this study site or the loess-related slope failures in general. On the basis of aerial images (res. 5 cm), Digital Elevation Model (res. 10 cm), and field investigations, we analyzed the distribution and failure mode of the landslides in Heitai. The geological structure and characteristics of 69 landslides (vol. 5×10^3–6×10^6 m^3) are studied. The preliminary results of groundwater recharge in the terrace and formation of the apparent spring lines on the slope surface are analyzed to better understand the failure modes. We divided the landslides in Heitai into two groups based on the location of the failure surface, i.e. loess landslide and loess-bedrock landslide, of which the development is governed by the angle between the principle direction of slope deformation and the dip of bedrock bedding. We further analyzed the failure mode of each type observed in Heitai, defined as follows: loess-bedrock planar slide, loess-bedrock irregular slide, loess flowslide, loess slide, and loess flow. The proposed types of loess-related landslide are to be incorporated in the Varnes classification (Varnes, 1978) in consideration of the engineering properties of loess, and to provide backward compatibility for Heitai and potentially other regions in the Loess Plateau of China.

1. Introduction

The Heitai terrace is formed by the fourth river terrace of the Yellow River in Gansu Province, China (Fig. 1a). More than 50 gullies are formed at the edge of the terrace. The terrace has a surface area of 9 km^2 with the maximum length of 5.2 km (W–E) and a width of 2.5 km (N−S). It is part of the Heifangtai terrace with high concentration of loess-related landslides due to surface irrigation started in 1968 (Derbyshire, 2001; Peng et al., 2016; Zeng et al., 2016; Zhou et al., 2014). Loess slope failure is common upon wetting due to its high porosity and collapsibility (Dijkstra et al., 1994; Jiang et al., 2014; Liu et al., 2016; Smalley et al., 2001; Wu et al., 2017; Yuan and Wang, 2009). Irrigation provides 4–6 cycles of groundwater recharge annually, which has increased the groundwater level by 20 m at an average rate of 0.18 m yr^{-1} (Xu et al., 2014) and caused about 200 landslides along the edge of the terrace (Fig. 1b). Study on the loess-related landslides in Heitai sustained its popularity due to frequent failures and significant societal impacts.

Landslide classification system forms a long-lasting research topic (Alimohammadlou et al., 2013; Casagrande, 1940; Cruden and Varnes, 1996; Görüm et al., 2011; Hungr et al., 2011; Hungr et al., 2014; Hutchinson, 1988; Qi et al., 2010; Varnes, 1978; Wang and Zhou, 1999; Xu et al., 2016). In many cases, defining the landslide type serves as a 'baseline' of the problem because it reflects the landslide material and behavior (Hungr et al., 2014). Landslides in loess provide a unique collection of landforms and failure mechanisms that are often undervalued in the global classification systems. Loess is recognized as a unique material, created by aeolian deposition in the Loess Plateau of China, comprising predominantly silt-sized particles that form cemented meta-stable structures with characteristically high void ratios. Landslides in loess are often generalized as a single type of landslide based on the material composition, such as loess flow by Varnes (1978), and loess flowslide by Hungr et al. (2014), under the category of earth flow. In the context of landslide behavior, loess-related slope failure was divided into different types based on either the movement and failure mechanism or the location of the failure surface. For example,
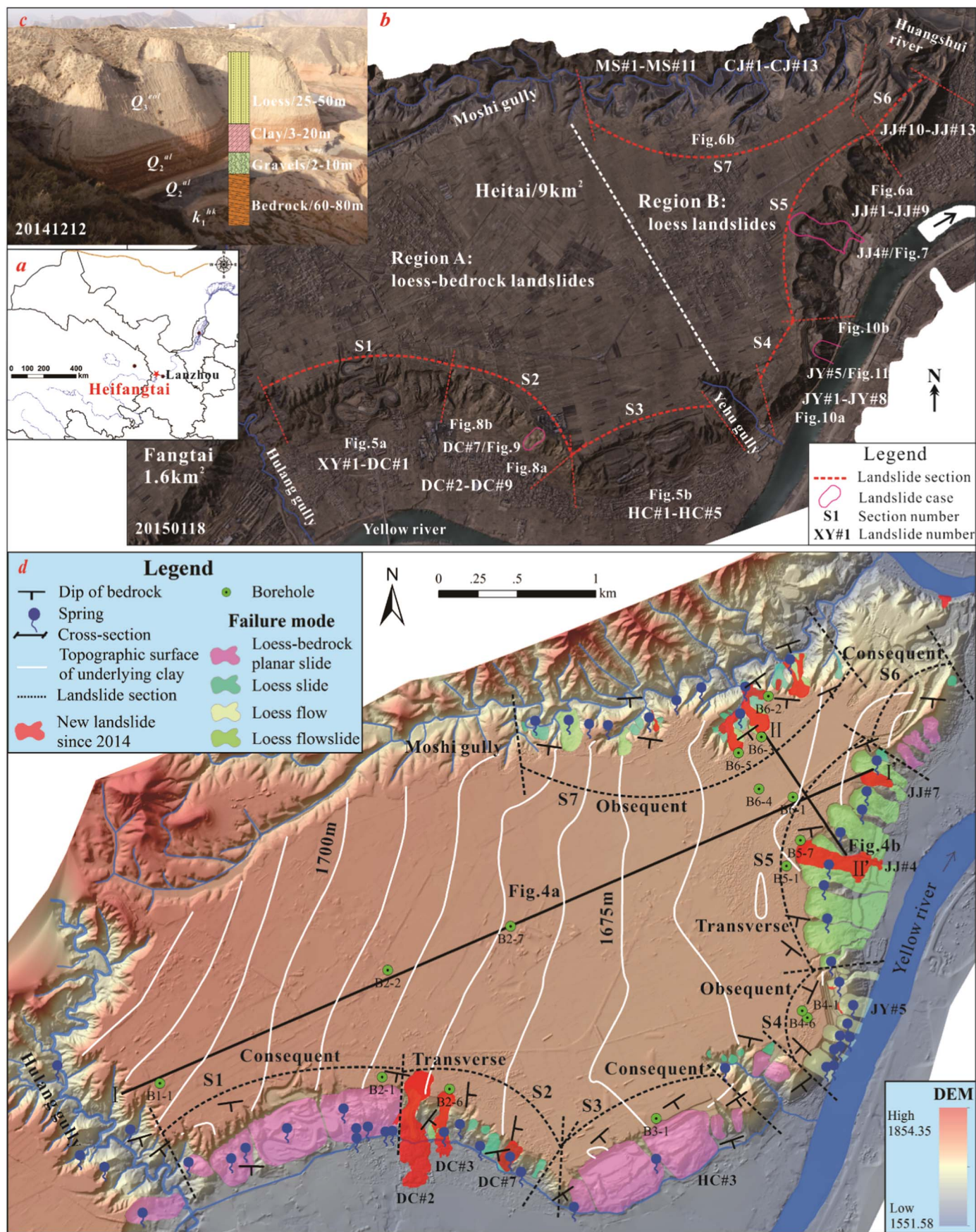
Fig. 1. (a) Location of the study area; (b) Aerial view of the Heifangtai terrace with landslide sections (image taken on Jan 18, 2015); (c) Lithological profile of Heitai; (d) DEM of Heitai with geological setting, distribution of surface seepage, and contour of the upper surface of the clay layer. Bedrock dip, borehole and well locations, ERT survey lines, and geological profiles are indicated.

Table 1

Landslide classifications for loess-related slope failures in Heifangtai and the Loess Plateau of China.

Type of landslides		Descriptions and definitions (if provided)		
Material	Movement			
Loess	landslide	• A board definition for landslide involves primarily loess; • A common type of landslide in Heifangtai and other loess regions in China; • Landslide develops within loess and/or contains fractions of mudstone(Wu and Wang, 2002); • Landslide develops in loess and it is typically accompanied by fluidization and liquefaction (Wang et al., 2004); • *Asequent landslides* (Meng and Derbyshire, 1998): landslides developed exclusively in loess;	Loess Plateau	
	slide	• In general, such type of failure has small scale and short runout; • *Collapse -sliding* (Lu, 1984; Zhou et al., 2002): collapse with subsequent sliding motion; • *Tan -ta* (Meng and Derbyshire, 1998): small adjustment failures due to localized changeswith no clear failure plane; • *Loess slide* (Wu and Wang, 2002): failure develops in loess containing layers formed at different ages, sliding surface is governed by vertical joints; • *Loess slide -fall* (Xu et al., 2009) or *loess slide* (Xu et al., 2008; Xu et al., 2014) : failure develops in the unsaturated portion of the loess slope with shallow thickness, small scale, short runout, and uniform color of deposit;	Loess Plateau Heifangtai	
	flow	• Most of the failures exhibit fluidized movement with long runout and high speed; • *High -speed collapsing landslide* (Zhao et al., 1995): failures with catastrophic fall and slide, with smooth scarp after numerous failures; • *Loess earthflow* (Xu et al., 2008) or *loess flow* (Xu et al., 2009; Xu et al., 2014) : failure initiates at thecontact between loess and the underlying clay in Heitai. Surface seepage can be seen at the failure site with steep scarp (ave 35 m). The movement lasts for <1 min, exhibiting liquefaction and fluidization with high-speed and long runout (>300 m). The perched water table at the concave topography is higher than the other natural platform borders under irrigation conditions, causing recurring failures;	Loess Plateau Heifangtai	
Loess -Bedrock	interface landslide*	• *Bedrock contact landslide* (Meng and Derbyshire, 1998): sliding of loess along the bedrock surface, often due to a saturated base with progressively decreasing strength by groundwater stagnation at the interface; • *Loess interface landslide* (Wu and Wang, 2002): common at slopes with the average gradient of 10°-20°, strain-softening occurs at the interface of loess and bedrock forming the sliding surface; • *Loess -mudrock interface landslide* (Xu et al., 2008): the principal sliding direction aligns with the bedrock dip causing sliding surface develops along the mudstone parting and causing lowvelocity failure, it is often recurring and forms step-shaped head of deposits;	Loess Plateau Heifangtai	• A board definition for landslide with failure surface develops in the overlaying loess layer and propagates into the underlying bedrocks; • A common type of landslide in Heifangtai and other loess regions in China; • *Loess -bedrock landslide* (Xu et al., 2009): Presents large-scale accumulation landform; has a short runout; rear part of landslide body has obvious dip-slip phenomena
	plane landside	• *Low -speed landslide along weak structural belt* (Zhao et al., 1995): groundwater flow along joints and bedding plane reduces strength and resistance to deformation, and eventually causes creeping like low-velocity landslide. • *Loess -mudstone plane landslide* (Wu and Wang, 2002): occurs in bedding plane with mild dip (10°-20°) under long-term gravitational deformation causing shear failure along bedding plane; • *Loess -bedrock landslide* (Wang et al., 2004): long-term deformation in the bedding plane due to strength reduction caused by groundwater, commonly has short runout and low-velocity; • *Loess -mudrock bedding landslide* (Xu et al., 2008) or *Combined loess and bedrock along bedding planes* (Xu et al., 2014) : failure along the bedding plane has travel distance of 30-60 m at a speed of 0.002-0.005 m/s, it does not consist of the interface between covering loess and underlying clay;	Loess Plateau Heifangtai	• *Mixed landslide* (Meng and Derbyshire, 1998): ingress of groundwater through joints into the underlying bedrock, causes slope to failure, with no evidence of movement in the overlying loess layer;
	cutting landslide	• *Terrace landslide* (Meng and Derbyshire, 1998)**: it denotes to a special type of failure occurs along terrace margins, with slip surface develops within the loess, resulting in catastrophic failure under the impact of groundwater movements; • *Loess -mudstone cutting landslide* (Wu and Wang, 2002): The sliding body is mainly composed of loess and Middle Cenozoic strata. The main scarp is steep with size >1×10⁶ m³. • *Loess -bedrock incising landslide* (Xu et al., 2008) or *Combined loess and bedrock across bedding planes* (Xu et al., 2014): Slip surface cuts bedding planes with a high angle. Field survey shows that the difference between bedding plane dip and the sliding direction is 60°-90°.	Loess Plateau Heifangtai	Loess Plateau Heifangtai

*Loess-bedrock interface landslide is sometimes classified as a type of loess landslide as the deposit consists of mainly loess; we categorized such failure into the loess-bedrock landslide group because the deposit still contains other material, commonly clay and gravel.

**The concept of terrace landslide was formulated to generalize the large-scale and high-speed landslide occur at the loess terrace margin; but the definition and character descriptor of terrace landslide is similar to the loess-bedrock cutting landslide.

*Loess-bedrock interface landslide is sometimes classified as a type of loess landslide as the deposit consists of mainly loess; we categorized such failure into the loess-bedrock landslide group because the deposit still contains other material, commonly clay and gravel.

**The concept of terrace landslide was formulated to generalize the large-scale and high-speed landslide occur at the loess terrace margin; but the definition and character descriptor of terrace landslide is similar to the loess-bedrock cutting landslide.

Lu (1984) classified loess-related landslides into slow-gliding landslide and collapse-gliding landslide, and Zhou et al. (2002) classified them into loess landslide and loess-paleosol landslide. Meng and Derbyshire (1998) provided the first systematic evaluation on the types of loss-related landslide in Gansu Province, categorized them based on the location of the failure surface, i.e. bedrock contact landslides, paleosol contact landslides, mixed landslides, loess landslides, terrace landslides, and Tan-ta. Wu and Wang (2002) and Xu et al. (2008) combined the character descriptors of landslide movement and sliding surface and performed a systematic evaluation for the Heifangtai terrace.

Several loess-related landslide classification systems have been introduced to scrutinize the failures in Heifangtai but there is no unanimous agreement on the landslide types (Table 1). Since the definitions and descriptions in different classifications were formulated by using case studies from different part of the Loess Plateau, the usage of the terms for the landslide type can be ambiguous or misleading, and often contradicts with other systems even for the same study area. To accommodate all types of loess-related landslides in Heitai and potentially other regions in the Loess Plateau, we classified the slope failures into two groups based on the material composition, i.e. loess landslide and loess-bedrock landslide, and divided them into 5 types using character descriptors based on the failure modes, movement types and failure surface developments.

Discussions on the landslide classification focus on the types encountered in Heitai, but they are formulated in a concise way to potentially incorporate all types of loess-related slope failures in the Loess Plateau. The main objectives of this note are to investigate the spatial distribution of landslides in the Heitai terrace, and to classify the landslide types and failure modes. The landslide types introduced here is not to devise a new classification system or to modify the existing Varnes classification (Varnes, 1978), but to better characterize the loess-related failures in Heitai into more specific types under the framework of the updated Varnes classification (Hungr et al., 2014).

2. Study area

The tectonic activity in the study area was intense and resulted in multi-staged terraces under erosion. Surface runoff resulted in several major gullies in Heitai, such as the Hulang Gully and Moshi Gully, eroding into the bedrock, with an average height of 130 m and a gradient of 50–60°. Landslide deposit accumulates at the lower part of the slope at the edge. The Heitai terrace consists of four layers in the sequence of loess, clay, gravel, and bedrock (Fig. 1c). The top layer is Malan loess (Q_3^{eol}) with a thickness of 30–50 m, which is mainly composed of silt-sized loess with high porosity and open-paced fabric, resulting in high susceptibility to collapse upon wetting. Vertical and

Table 2
A summary of the landslides in Heitai terrace.

Section	Site	L	H	V	Φ_1	Φ_2	Φ_3	K	θ_1	θ_2	Type
		m	m	$10^4\,m^3$	°	°	°		°	°	
S1	XY#1	173.96	43	73.02	13.88	62.23	10.48	0.01	123.82	140	1
	XY#2	282.75	85	223.73	16.73	58.68	13.51	0.01	149.48	187	
	XY#3	345.55	70	523.68	11.45	53.85	10.62	0.04	155.56	172	
S2	DC#1	318.9	111	531.61	19.19	51.64	18.12	0.03	170.04	190	
	DC#2	346.09	106	32.03	17.03	32.65	14.78	0.29	165.52	135	2
	DC#3	293.48	104	77.32	19.51	51.84	17.25	0.31	195.45	96	
	DC#4	99.48	75	3.11	37.01	32.13	37.33	0.05	220.83	170	3
	DC#5	61.14	43	2.73	35.12	57.62	33.25	0.17	213.85	170	
	DC#6	156.37	101	19.15	32.86	46.78	31.88	0.12	209.26	135	
	DC#7	204.03	97	19.11	25.43	25.26	25.44	0.03	212.14	100	
	DC#8	132.26	90	7.9	34.23	58.09	31.18	0.13	208.79	100	
	DC#9	–	–	–	–	–	–	–	–	–	
S3	HC#1	244.32	101	77.04	22.46	32.44	19.92	0.13	149.5	140	1
	HC#2	386.18	104	553.05	15.07	32.83	11.96	0.05	153.06	165	
	HC#3	376.44	101	610.36	15.02	23.5	12.57	0.11	147.45	160	
	HC#4	130.4	58.7	6.2	24.24	41.07	22.29	0.14	164.03	170	
	HC#5	212.16	107	18.24	26.76	37.38	25.23	0.19	176.83	155	
S4	JY#1	226.15	132	28.68	30.27	30.01	30.39	0.1	126.21	164	4
	JY#2	181.41	121	7.05	33.7	35.48	33.15	0.2	123.28	270	
	JY#3	217.7	133	8.16	31.42	37.57	29.23	0.15	116.09	270	
	JY#4	163.31	108	5.26	33.48	41.95	32.55	0.14	106.51	270	
	JY#5	201.36	92	7.32	24.56	26.8	24.51	0.32	96.56	295	
	JY#6	342.2	113	8.69	18.27	65.63	16.96	0.54	78.75	217	
	JY#7	56.58	43	0.41	37.23	38.83	36.99	0.19	104.03	217	
	JY#8	88.26	57	0.94	32.86	56.74	28.17	0.19	109.93	217	
S5	JJ#1	353.43	121	34.38	18.9	55.64	16.18	0.09	76.45	217	2
	JJ#2	425.66	120	88.99	15.74	42.85	13.4	0.24	88.7	190	
	JJ#3	515.48	124	92.88	13.53	52.44	10.32	0.32	101.13	190	
	JJ#4	609.55	119	333.81	11.05	35.22	9.3	0.28	105.54	172	
	JJ#5	468.73	120	152.65	14.36	41.89	12.53	0.42	129.51	172	
	JJ#6	326.17	108	33.2	18.32	42.36	15.02	0.22	116.86	172	
	JJ#7	322.83	100	10.55	17.21	46.39	14.89	0.31	105.61	165	
	JJ#8	390.97	101	52.86	14.48	37.48	12.52	0.35	112.85	165	
	JJ#9	98.81	53	2.43	28.21	44.56	13.3	0.13	167.96	165	3
S6	JJ#10	190.56	91	6.89	25.53	42.58	24.79	0.33	143.04	1	1
	JJ#11[a]	178.63	70	6.17	21.4	48.77	19.66	0.09	135.02	166	–
	JJ#12	175.27	91	7.55	27.44	60.1	25.34	0.27	175.91	185	1
	JJ#13	45	50	2.08	48.01	44.22	49.04	0.06	120.25	195	3
S7	CJ#1	175.02	72	2.34	22.36	55.52	20.46	0.07	12.28	155	
	CJ#2	91.13	52	1.77	29.71	46.03	28.81	0.11	303.3	155	
	CJ#3	283.86	104	55.65	20.12	48.1	17.1	0.33	350.39	166	2
	CJ#4	164.11	99	17.75	31.1	64.36	28.99	0.28	354.94	166	3
	CJ#5	207.58	79	15.77	20.84	52.65	18.66	0.1	273.82	155	
	CJ#6	199.53	64	29.92	17.78	48.11	14.53	0.49	317.12	155	2
	CJ#7	129.12	54	5.99	22.69	72.59	16.25	0.13	336.4	155	3
	CJ#8	154.97	40	15.91	14.47	59.27	7.96	0.21	328.87	145	2
	CJ#9	80.23	31	3.36	21.13	35.09	16.26	0.13	275.73	145	3
	CJ#10	–	–	–	–	–	–	–	50.68	145	
	CJ#11	62.43	38	0.82	31.33	49.1	13.56	0.23	114.46	166	
	CJ#12	57.28	39	0.55	34.25	34.94	33.87	0.49	118.74	166	
	CJ#13	40.84	40	0.16	44.4	54.38	39.72	0.22	120.07	166	
	MS#1	41.18	36	0.69	41.16	57.11	39.66	0.13	226.43	165	
	MS#2	21.43	12	0.36	29.24	61.93	20.46	0.19	304.64	165	2
	MS#3	57.57	28	1.59	25.94	74.2	17.34	0.16	11.03	166	
	MS#4	32.93	13	0.24	21.54	38.44	18.93	0.05	12.75	177	
	MS#5	48.3	21	0.94	23.5	55.48	14.87	0.14	35.45	177	3
	MS#6	78.69	43	2.78	28.65	53.91	26.07	0.08	330.92	177	
	MS#7	81.66	33	3.67	22	50.7	16.85	0.12	322.88	177	
	MS#8	185.66	34	8.46	10.38	49.44	5.67	0.28	334.44	177	2
	MS#9	250.81	59	25.87	13.24	48.4	10.69	0.25	355.34	188	
	MS#10	76.99	43	4.05	29.18	73.77	19.21	0.17	15.02	188	3
	MS#11	22.8	25	0.81	47.64	54.89	45.19	0.06	67.51	188	

ARTICLE IN PRESS

D. Peng et al.   Engineering Geology xxx (xxxx) xxx–xxx

Table 2 (*continued*)

Section	Site	L	H	V	Φ_1	Φ_2	Φ_3	K	θ_1	θ_2	Type
		m	m	$10^4\ m^3$	°	°	°		°	°	

Note Type 1: loess-bedrock planar slide; 2: loess flowslide; 3: loess slide; 4: loess flow.
  [a] JJ#11 is a loess-bedrock irregular slide.

sub-vertical joints are well developed in the loess layer providing conduits for groundwater recharge. The underlying clay layer (Upper Pleistocene) has a thickness of 3–20 m varying from NW to SE of the terrace; it can be considered as an impermeable layer due to its low permeability. The clay layer overlies a layer of gravel with thickness of 1–10 m consists of gravel, quartz, and granite. The bedrock comprises sandstone with mudstone partings (Lower Cretaceous) which has the bedding plane dipping 135°∠11°. The thickness of the exposed rock stratum is > 70 m. The apparent spring lines are visible at the bedrock slope along the edge of the terrace.

Landslides are reconstructed by using the high-resolution Digital Elevation Model (DEM) of the Heitai terrace. Unmanned Aerial Vehicles (UAVs) and 3-D Laser Scanning were used to create the DEM at a resolution of 10 cm. A typical UAV mission involves 35 flights spans over one week. Each image is processed in the form of high precision 3-D point clouds constrained by 15 primary control points (forming 13 triangulation nets) and 146 ground control points (GCPs) in the study area. The construction of DEM was calibrated by the ground GPS stations, and the precision of the DEM data was enhanced by the high-resolution aerial images.

A total of 69 landslides were identified and tabulated in Table 2; seven of the landslides are located in the Yehu Gully and the rest are found along the edge of the terrace (Fig. 1d). The group of loess landslide denotes to the slope failure occurred entirely within the loess layer, and the group of loess-bedrock landslide is referred to the landslide with failure surface originated from the loess layer and extended into the underlying bedrock layer (either cutting through or along the bedding plane). We divided the terrace into Region A (R_A) and Region B (R_B) based on landslide group (Fig. 1b). The landslides in R_A are loess-bedrock landslides (vol. 1×10^5–$6 \times 10^6\ m^3$), while the landslides in R_B are loess landslides (vol. 5×10^3–$2 \times 10^6\ m^3$). We further divided R_A and R_B into 7 sections, i.e. S1 (Xinyuan), S2 (Dangchuan), S3 (Huangci), S4 (Jiaojiaya), S5 (Jiaojianan), S6 (Jiaojiabei), and S7 (Moshigou), based on the included angle, α between the principal sliding direction of the landslide and bedrock dip (Fig. 2). The included angle governs the landslide groups and categorizes the slopes as consequent slope ($\alpha < 30°$), transverse slope ($30° \leq \alpha \leq 90°$), and obsequent slope ($\alpha > 90°$). Loess landslides are developed on the transverse slopes (S2 and S5) and obsequent slopes (S4 and S7), whereas loess-bedrock landslides are distributed on the consequent slopes (S1, S3, and S6). The bedrock dip of transverse slope is nearly perpendicular to the direction of slope deformation, which obstructed the potential sliding motion along the dip of the bedrock bedding. As shown in Fig. 2, the primary sliding direction of the loess-bedrock landslides and
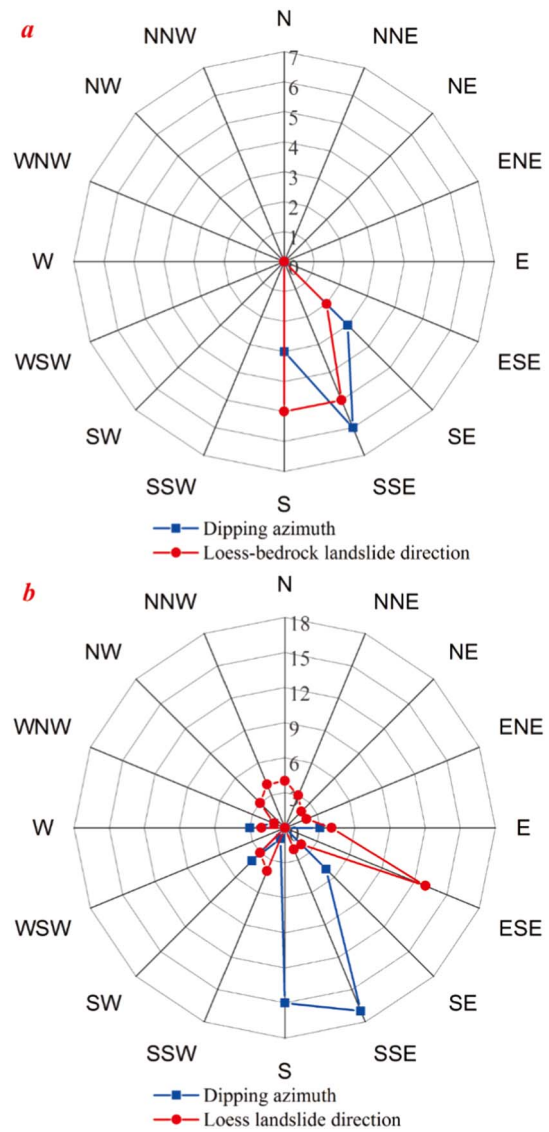
Fig. 2. The relations between the dip of bedrock bedding planes and sliding direction of landslides. (a) dip of the bedding plane and directions of loess-bedrock landslides; (b) dip of the bedding plane and directions of loess landslides.
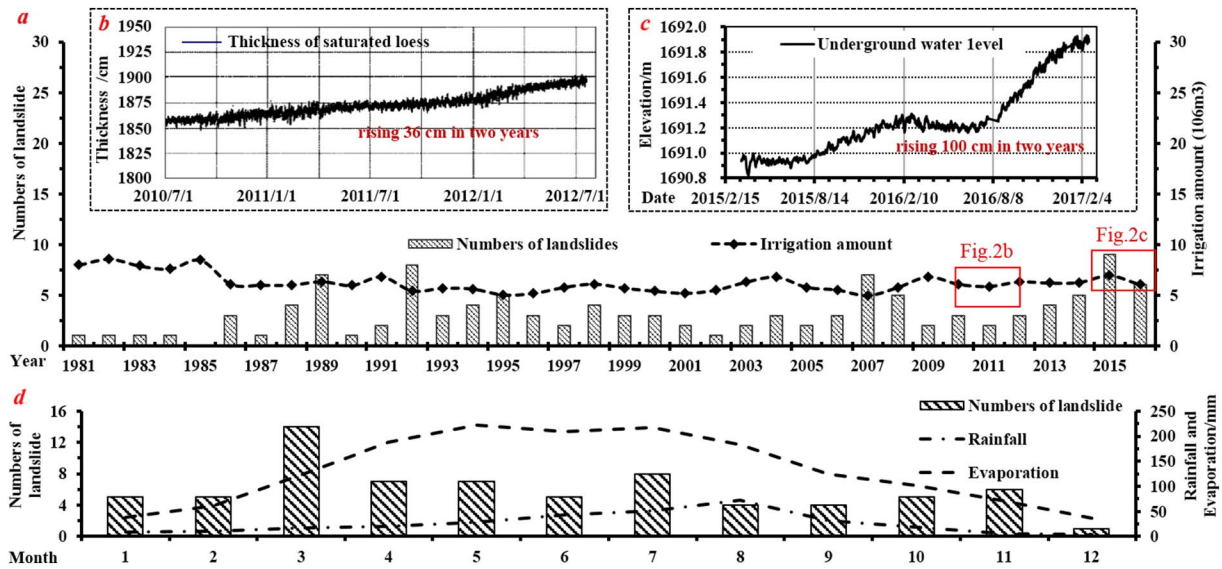
Fig. 3. Relations of irrigation, groundwater variations, precipitation, evaporation, and landslides. (a) Annual variations of landslide occurrences and irrigation; (b) Changes in the thickness of the saturated loess layer in B6-3 (location see Fig. 1d) (Xu et al., 2014); (c) Changes in the groundwater level in B6–1 (location see Fig. 1d); (d) Monthly average of landslide events, rainfall, and evaporation before 2012 (Wei, 2012).

bedrock dip are orientated about 170°, but that of the loess landslide and bedrock dip forms an average difference of nearly 60°. Such phenomena indicate strong influence of the bedrock dip on the development of the landslide.

The alluvial clay layer has a nearly uniform thickness and low permeability (Fig. 1d), which results in a saturated base in the overlaying loess layer. The long-term irrigation increased the groundwater level in the terrace by 0.36 m between Jul 2010 and Jul 2012, and by 0.5 m between Sept 2015 and Dec 2016 (Fig. 3b and c). The annual evaporation is three times greater than the precipitation (Fig. 3d). The rising groundwater is postulated as the main reason for the landslides in Heitai, where saturation of the base of the loess layer results in strain-softening of loess and reduces the resistance to the slope movement (Qi et al., 2017; Xu et al., 2011). Annual variations on the number of landslides are not well understood and out of the scope of this note (Fig. 3a). However, there is a somewhat temporal correlation, with a degree of lag, between landslide occurrences and irrigation activities in the terrace.

The distribution and dynamic groundwater is a key factor in understanding the distribution of landslides in Heitai. Groundwater level in the study site was mapped by using field data from 6 monitoring wells and 2 profile lines from the electrical resistivity tomography (ERT) survey across the east part as well as the longitudinal center of the terrace (Fig. 4). The 2-D resistivity images of the subsurface water content were produced from a detecting line (segment length 300 m) with 61 steel electrodes at 5 m spacing. In consideration of the overall length of the survey lines (> 1 km and 5 km, respectively), effective depth of detection, and accuracy of the results, each segment of the profile line has an overlap of 100 m. Each measurement takes about 90 min and was repeated three times. The coordinates of electrodes were calibrated by ground GPS to ensure a straight line on the same profile with precise elevation. Well data were used to validate the ERT survey, which indicated a margin of error of ± 0.5 m for the groundwater level variation, and the apparent spring lines on the slope surface confirmed the groundwater mapping results. The ERT survey shows that the groundwater level is higher on the west of the terrace with the maximum elevation difference of 30 m (Fig. 4a). In the profile line II-II′, the groundwater level dropped along the slope geometry of the cut

slopes in S5 (Fig. 4b), of which the variations play a critical role in the landslide types in S5.

3. Landslide types and failure modes

We classified landslides in Heitai into 5 types, and their definitions and character descriptors are as follows:

1. *Loess-bedrock planar slide*: failure surface develops in the loess layer and propagates into the underlying bedrock resulting in failure along the bedding plane. It is typically a large-scale failure with short runout and low internal concavity. Cracks and faults can be observed in the accumulation body.
2. *Loess-bedrock irregular slide*: failure surface develops in the loess layer and propagates into the underlying bedrock resulting in sliding on an irregular failure surface exploiting discontinuities in the bedrock that are possibly separated by segments of intact rock.
3. *Loess flowslide*: failure surface develops entirely within the overlying loess layer. It is a large-to-medium scale failure with rapid movement and long runout exhibiting liquefied and fluidized flow behavior. Such failure type has a higher K (average 0.26).
4. *Loess slide*: failure surface develops entirely within the overlying loess layer. Such failure has a smaller size and shorter runout with failure surface commonly seen in the unsaturated part of the loess layer. It usually occurs at the locations with widely distributed cracks and joints.
5. *Loess flow*: failure surface develops entirely within the overlying loess layer. Such failure is only seen after slope-cutting at certain locations in Heitai. The failure is relatively small with short runout exhibiting slurry-like flow behavior.

A conceptual failure mode is depicted for each type to illustrate the failure process. Analysis on the loess-bedrock irregular slide is limited as only one irregular slide was identified in Heitai (see Table 2), and thus the discussion on such failure mode is not included in this note.
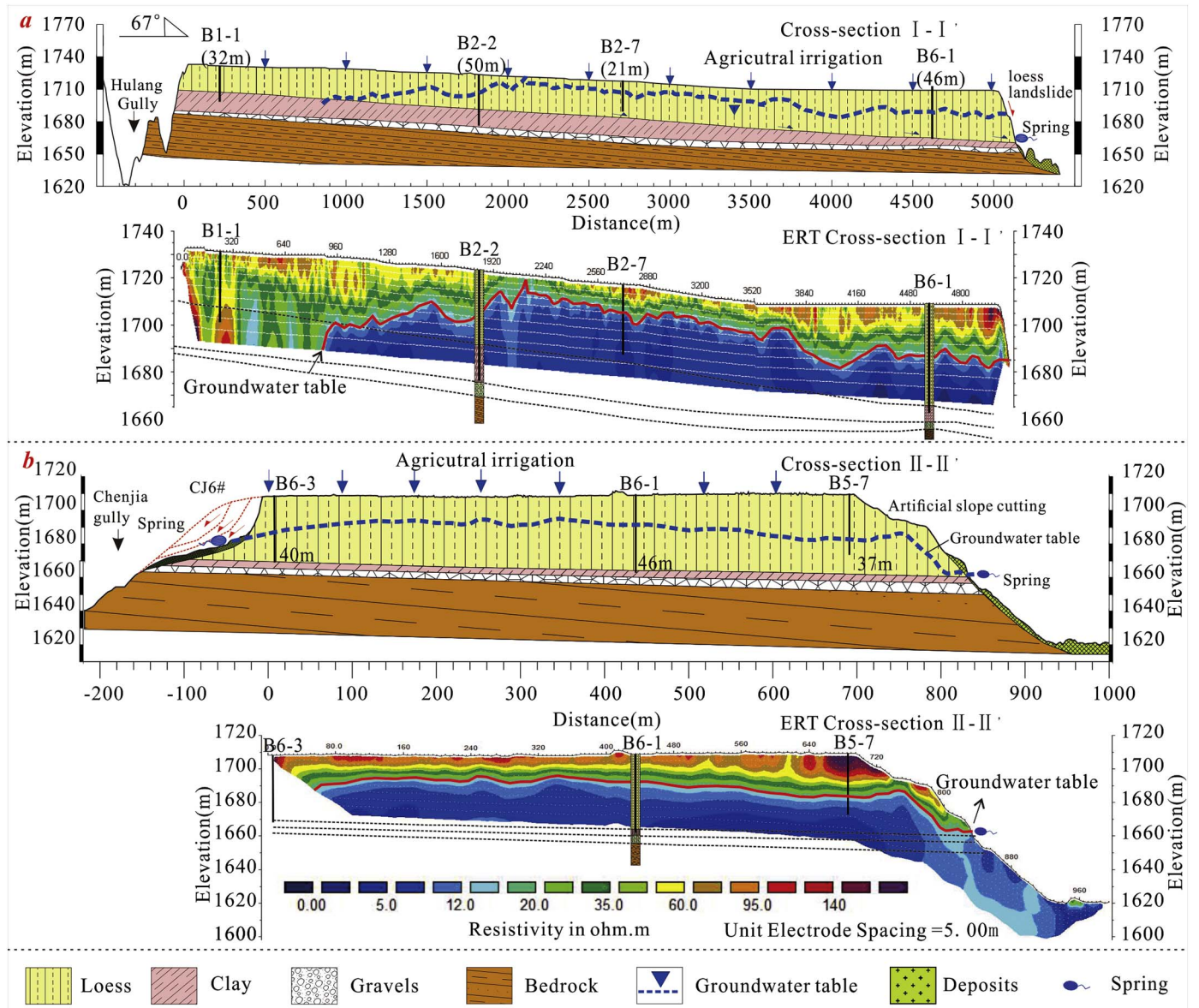
Fig. 4. Electrical resistivity map and geological cross-section across the east part and the longitudinal center of the terrace. (a) Variations of groundwater table in Heitai (from SW to NE); (b) Groundwater table next to JJ#4 showing significant drop after slope cutting in S5. Profile locations see Fig. 1d.

3.1. Loess-bedrock planar slide

A total of 12 loess-bedrock landslides are found in R_A, of which the failure surfaces originated in the overlaying loess layer and developed along the bedding plane in the consequent slopes with a dip of $190°\angle 11°$ in S1 and $160°\angle 10°$ in S3. The principal sliding direction of the landslide align with the dip of the bedrock. The volume of the loess-bedrock landslide ranges 6×10^4–6×10^6 m^3 with an average of 2.2×10^6 m^3. Geometrical characteristics of the planar slides are presented in Fig. 5. In the absence of field data on the travel velocity, interviews with the local inhabitants confirmed that slow (0.002–0.005 m/s, according to Xu et al., 2014 for the corresponding type) with short runout (< 30 m).

This landslide type and its failure mode is illustrated in Fig. 5 and an example is the HC#3 landslide in S3. The HC#3 loess-bedrock landslide occurred on Jan 30, 1995 (vol. 6×10^6 m^3), and followed by another failure at the same location on May 14, 2006 (vol. 3×10^6 m^3). The

entire failure process in 2006 spanned over 90 mins with an estimated travel velocity of 0.005 m/s and a runout of 30–60 m. The scarp of HC#3 retreated over 10 m as the second landslide developed at the previous site. A multi-level terrace was formed on the slope after the failures.

The seepage of groundwater on the slope surface results in the apparent spring line above the alluvial clay layer as well as on the bedrock slope, indicating a saturated basal zone in the overlying loess layer and groundwater infiltrations along the bedding plane of the bedrock. Cracks are firstly formed at the surface of the terrace, and are likely to be caused by 1) the deformation of the saturated base of the loess layer and 2) unloading due to the preceding landslides. The cracks subsequently propagate from the overlaying loess layer to the bedrock forming the failure surface. Field evidence of the surface cracks is shown in Fig. 5. As deformation continues and cracks propagate into the bedrock, it provides flow passage for the ingress of groundwater along the bedding plane, which erodes the bedrock reducing resistances

Type	Statistical parameter	V	Φ_1	Φ_2	Φ_3	K
Bedrock slide	max	610.36	27.44	62.23	25.34	0.33
	min	6.17	11.45	23.5	10.48	0.01
	Average	219.79	19.93	45.43	17.87	0.11
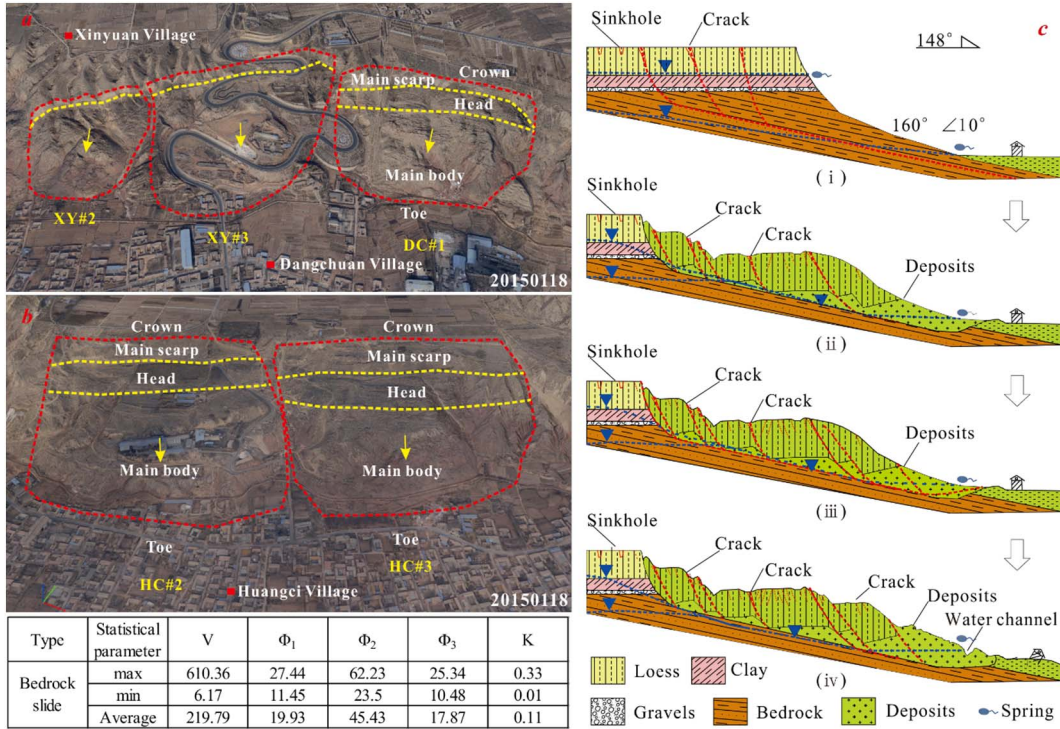
Fig. 5. Loess-bedrock planar slide. (a) slides in S1; (b) slides in S3; (c) Failure model of loess-bedrock planar slide. Geometric characteristics of planar slides are tabulated. Landslide locations see Fig. 1b.

Type	Statistical parameter	V	Φ_1	Φ_2	Φ_3	K
Loess flowslide	max	333.81	29.24	74.2	20.46	0.49
	min	0.24	10.38	35.22	5.67	0.05
	Average	58.58	17.27	48.88	13.55	0.26
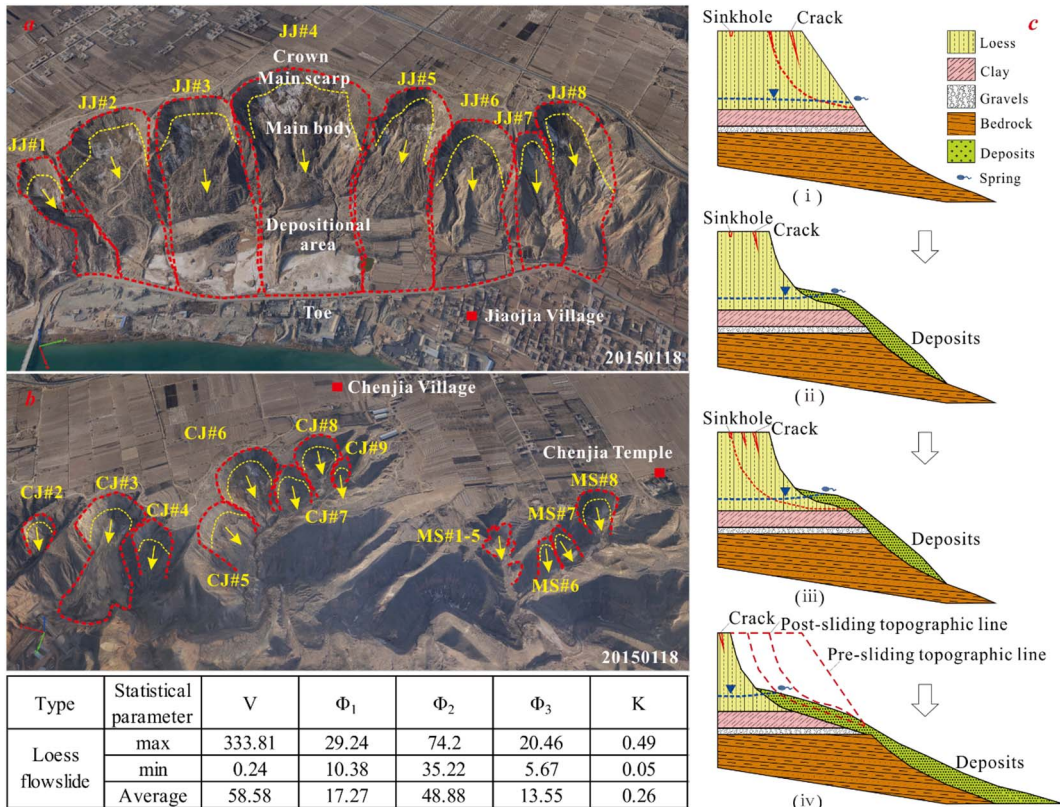
Fig. 6. Loess flowslide. (a) flowslides in S5; (b) flowslides in S7; (c) failure mode of loess flowslide showing retrogressive behavior resulted in significant slope retreat along the edge of Heitai. Geometric characteristics of flowslides are tabulated. Landslide locations see Fig. 1b.
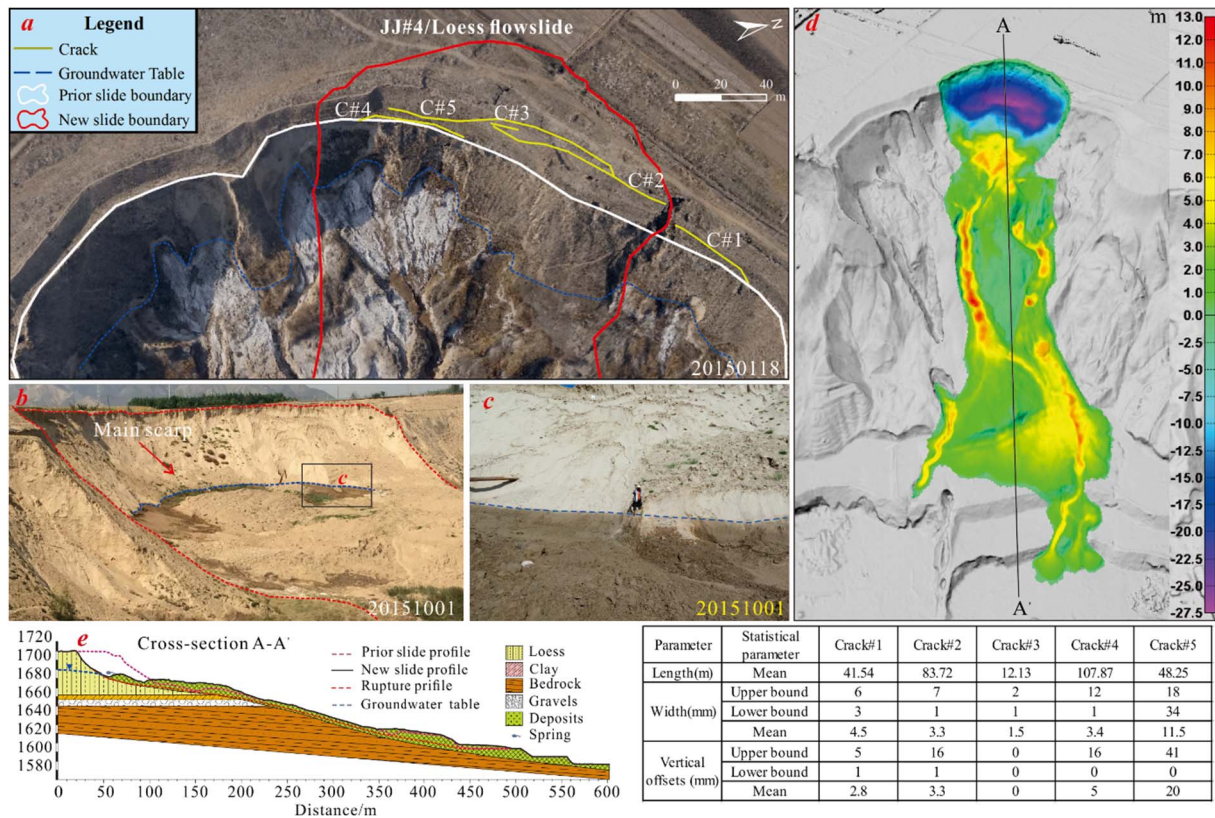
Fig. 7. JJ#4 loess flowslide in S5 (location see Fig. 1b). (a) Crown cracks, groundwater discharge, and landslide scarp boundaries (image taken on Jan 18, 2015); (b) A large amount of groundwater seepage 'washes' fine particulars in loess forming salt coating at the bottom of the main scarp (image taken on Oct 1, 2015). (c) Evident boundary between the landslide scarp and saturated deposit; (d) Surface elevation change of the loess flowslide estimated by using the pre- and post-failure DEMs; (e) geological profiles of JJ#4. Pre-sliding (occurred on Jan 26, 2015) crown cracks are summarized and tabulated.

in the discontinuities and leads to slope deformation and failure.

3.2. Loess flowslide

The loess flowslide is the most pronounced type of landslide in Heitai due to its high velocity, long runout, and far-reaching impacts. A total of 14 loess flowslide occurred in S5 and S7 since 2014, where the slope has a height of loess layer over 40 m with a slope gradient of 50°–70°. The volume of the loess flowslides are 2×10^3–3×10^6 m^3 with an average of 6×10^5 m^3.

The failure mechanism of loess flowslide is analyzed in detailed by Qi et al. (2017). As illustrated in Fig. 6, the failure surface was developed entirely within the loess layer. The retrogressive behavior typically involves a two-staged failure process associated with the groundwater flow in the terrace as well as behind the backwall of the preceding failure. At the 1st stage, as the location of the apparent spring line indicates, groundwater saturates the base of the loess layer and discharges at the edge of the terrace. This leads to the collapse of the loess structure, which in turn, results in a progression of strain development in the overlying loess deposits. Post-peak shear strength is thus mobilized over an increasingly small area along the potential slip surface until failure of the remaining loess occurs. At this stage, the failure is small in volume occurring at a drained condition, but it intensifies the localized groundwater convergence behind the scarp, which increases the thickness of the saturated base and the pore-water pressure behind the scarp. With the displaced material being deposited above the apparent spring line, an undrained condition develops behind the scarp, where excess pore-water pressure may be induced by micro-shearing of collapsing void in the loess matrix (i.e. 2nd stage, defined by Qi et al., 2017), and it results in abrupt deformation and liquefied flow movement with long runout across a low-relief terrain. The retrogressive behavior of loess flowslide is likely to cause a new failure at the same location, and subsequently slope retreat by its very nature.

A large amount of groundwater seepage and salt coating can be seen at the head of the displaced material before failure, indicating saturation and the removal of fine particles in the loess element. The failure is exemplified by the JJ#4 flowslide as shown in Fig. 7. Surface cracks with a width of 1–18 mm and vertical offsets of 1–41 mm are common at the crown due to unloading from the previous failures.

3.3. Loess slide

The loess slides are located on the transverse slopes in S2, where the principal direction of the slope deformation is perpendicular to the bedrock dip, and thus the propagation of the cracks in the loess layer fail to continue into the underlying bedrock. Such type of landslide is shallow with a runout distance of 100–200 m and a volume of 1.6×10^3–7.7×10^5 m^3.

As shown in Fig. 8, similar to loess flowslide, saturation of the basal zone of the loess layer led to strain-softening and deformation. The unloading crown cracks are common prior to loess slide (Fig. 9), with width ranging from 5 to 420 mm and vertical offsets of 10–400 mm.

Type	Statistical parameter	V	Φ_1	Φ_2	Φ_3	K
Loess slide	max	77.32	48.01	73.77	49.04	0.49
	min	0.16	17.03	25.26	13.3	0.03
	Average	23.05	28.74	43.48	27.3	0.16
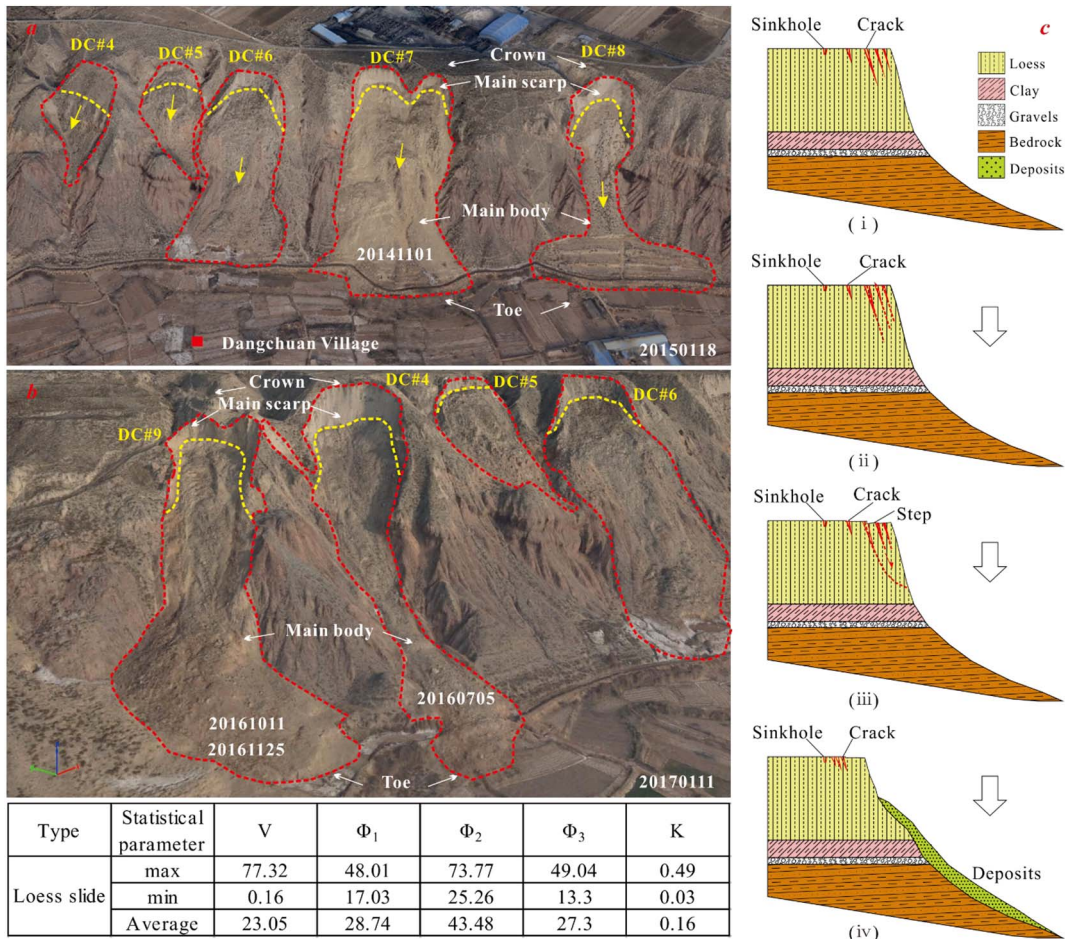
Fig. 8. Loess slide. (a) slides in S2; (b) slides in S2 showing new failure in DC#9; (c) Failure mode of loess slide showing the formation of crown cracks and failure. Geometric characteristics of slides are tabulated. Landslide locations see Fig. 1b.

The loess slides in S2 were rarely the focus of the landslide studies in Heitai, as they are considerably smaller compare to the loess-bedrock planar slide (S1 and S3) and the runout distances are significantly shorter compare to loess flowslide (S5 and S7). Apparent spring line can be observed for some loess slides, however there is no pronounced pre-/ post-failure variation in the groundwater associated with loess slide.

In the past three years, 7 loess slides occurred in S2 and S7; but recent failures at the previously known loess slide sites, i.e. DC#2 and DC#3, exhibited fluidization and liquefaction behavior during movement with long-runout and high-velocity, characters that are clearly associated with loess flowslide. It is postulated that the loess slide is capable to evolve into a more diffuse failure as the slope deformation and/or irrigation continues, or one may even argue that loess slide is the early form of a loess flowslide.

3.4. Loess flow

Slope cutting in S4 began in 2012 as an attempt to mitigate the slope deformation. Cutting alters the geometrical and stress conditions and reduces the rate and magnitude of slope deformation. However, it re-

sults in a different type of loess landslide exhibiting a more flow-like failure. The loess flow exhibits slurry-like movement at a much smaller velocity and magnitude. Such type is observed only on the engineered loess slopes in S4 (Fig. 10). The volume of the loess flow ranges from 4×10^3 to $2.9 \times 10^5 \, \text{m}^3$ with an average of $8.3 \times 10^4 \, \text{m}^3$, which is typically smaller than other types of landslide in Heitai.

Man-made excavation reduces the surcharge imposed on the slope, resulting in a more localized failure with comparatively smaller size of deposit. The loess flow may be ascribed to the drastic drop of groundwater level at the edge of the terrace as shown in Fig. 4, which generated a smaller hydraulic gradient between the scarp and flanks of the landslide (Fig. 10). Based on the role of groundwater and landslide deposit interaction analyzed for loess flowslide and loess slide, the size and volume of loess flow deposit is not sufficient to impede groundwater seepage at the edge to create an undrained condition, and thus no excess pore-water pressure can be generated at the failure state.

Loess flow typically occurs in the engineered slopes where the thickness of loess is 5–10 m. In the case of the JY#5 loess flow, field evidences in Fig. 11 shows a large amount of seepage and leaching of finer particles at the head of the deposit. Crown cracks have width of

Parameter	Statistical parameter	C1#	C2#	C3#	C4#	C5#	C6#	C7#	C8#	C9#	C10#
Length(m)	Mean	27.5	11.7	24.4	11	17.5	22.7	19.7	47.6	18.4	3.09
Width(mm)	Upper	312	97	107	86	46	55	67	38	428	68
	Lower	34	32	16	4	16	12	9	2	144	13
	Mean	170	51	39	47	26	23	37	18	267	34
Verfical offsets(mm)	Upper	543	148	159	3	22	0	86	67	743	-5
	Lower	0	2	0	0	-96	-76	0	0	343	-55
	Mean	232	71	41	1	-12	-15	17	16	483	-27
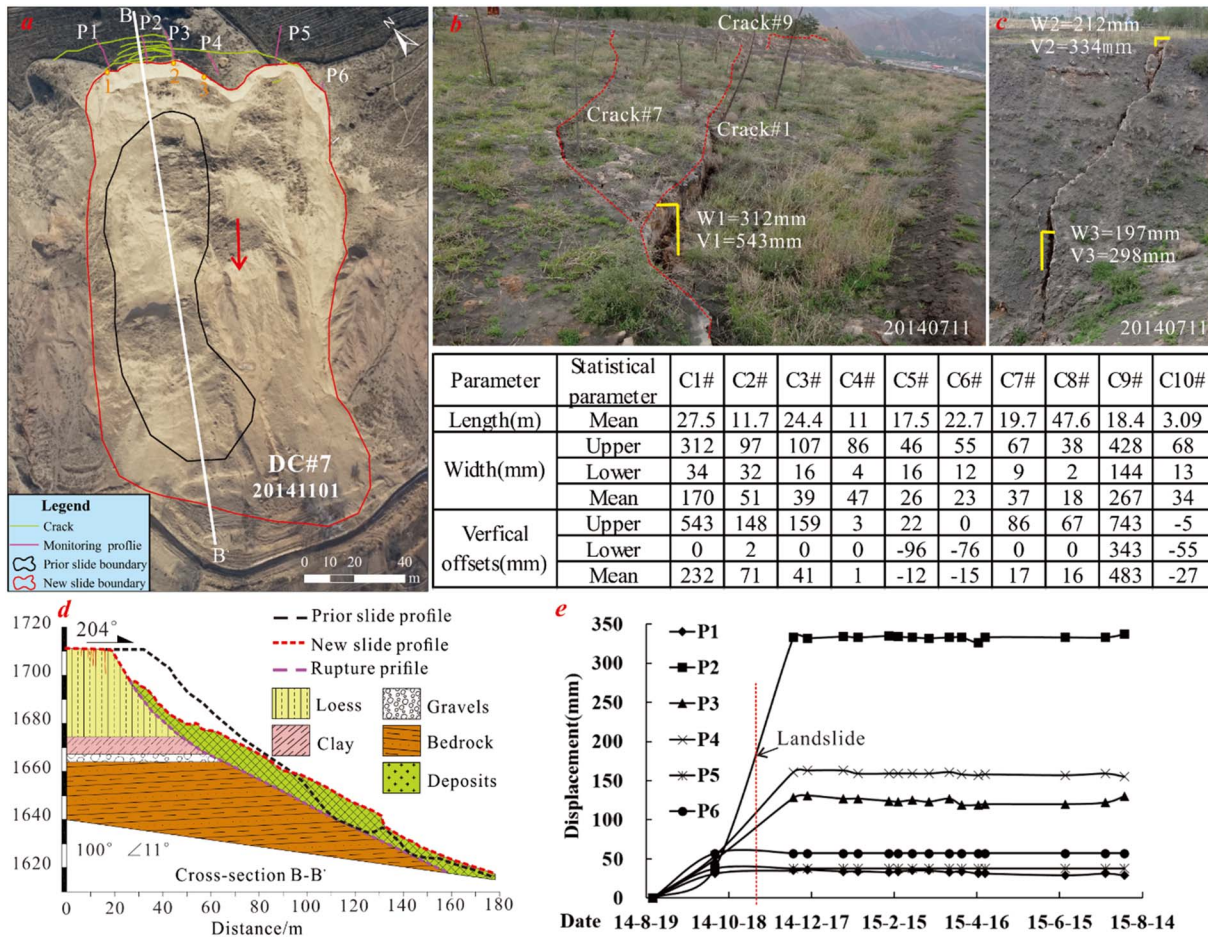
Fig. 9. DC#7 loess slide in S2 (location see Fig. 1b). (a) Crown cracks, groundwater discharge, and landslide scarp boundaries; (b) crown cracks; (c) cracks at the flank of the slide; (d) geological profiles of DC#7; (e) field monitoring on the crack deformation by measure relative changes of surface markers (Aug 24, 2014–Aug 1, 2015); Pre-sliding (occurred on July 19, 2014) crown cracks are summarized and tabulated.

20–600 mm with vertical offsets of 10–400 mm, which are accompanied by evident subsidence in the crown area and a slight bending motion that are similar to toppling failure. Loess flow in S4 is almost constant with no evident seasonal variation in the magnitude and velocity.

4. Conclusions

In this note, the effects of geological structure and groundwater on the loess-related landslides on Heitai terrace are investigated. Notwithstanding the influence of additional factors, such as chemical concentration variations in the loess matrix due to groundwater (Zhang et al., 2013) and freezing-thawing cycles (Ge et al., 2011), on the temporal distribution of the landslides on the terrace, the spatial distribution can be ascribed to the geological structure and groundwater variations. By analyzing the distribution and failure mode of the landslides in Heitai, we classified the landslide types into: loess-bedrock planar slide, loess-bedrock irregular slide, loess flowslide, loess slide, and loess flow. The landslide types introduced here better characterize the loess-related slope failures into more specific types under the framework of the updated Varnes classification.

The main conclusions are as follows:

1. A total of 69 landslides is located in 7 sections in Region A and B of Heitai. We divided the landslides into group of loess-bedrock landslides or loess landslide. The failure surface of the loess-bedrock landslide originates in the overlying loess layer and extends into the bedrock, whereas that of the loess landslide remains entirely within the loess layer. Most of the loess-bedrock landslides are concentrated on the consequent slope in R_A with slow movement and large volume, whereas most of the loess landslides developed in R_B.

2. The difference between the principal direction of slope deformation and bedrock dip, α of each section governs the landslide groups: 1) for $\alpha < 30°$, the failure surface is likely to propagate into the bedrock and cause failure along the bedding plane, resulting in loess-bedrock landslides (S1, S3, and S6); 2) for $\alpha > 30°$, the failure surface develops entirely within the loess layer resulting in loess landslides (S2, S4, S5, and S7).

3. Irrigation triggers landslides in Heitai. With the increasing groundwater level, landslides recur at the edge of the terrace showing an unclear temporal correlation at different sections with possible transformation of landslide types.

Type	Statistical parameter	V	Φ_1	Φ_2	Φ_3	K
Loess flow	max	28.68	37.23	65.63	36.99	0.54
	min	0.41	18.27	26.8	16.96	0.1
	Average	8.31	30.22	41.62	28.99	0.23
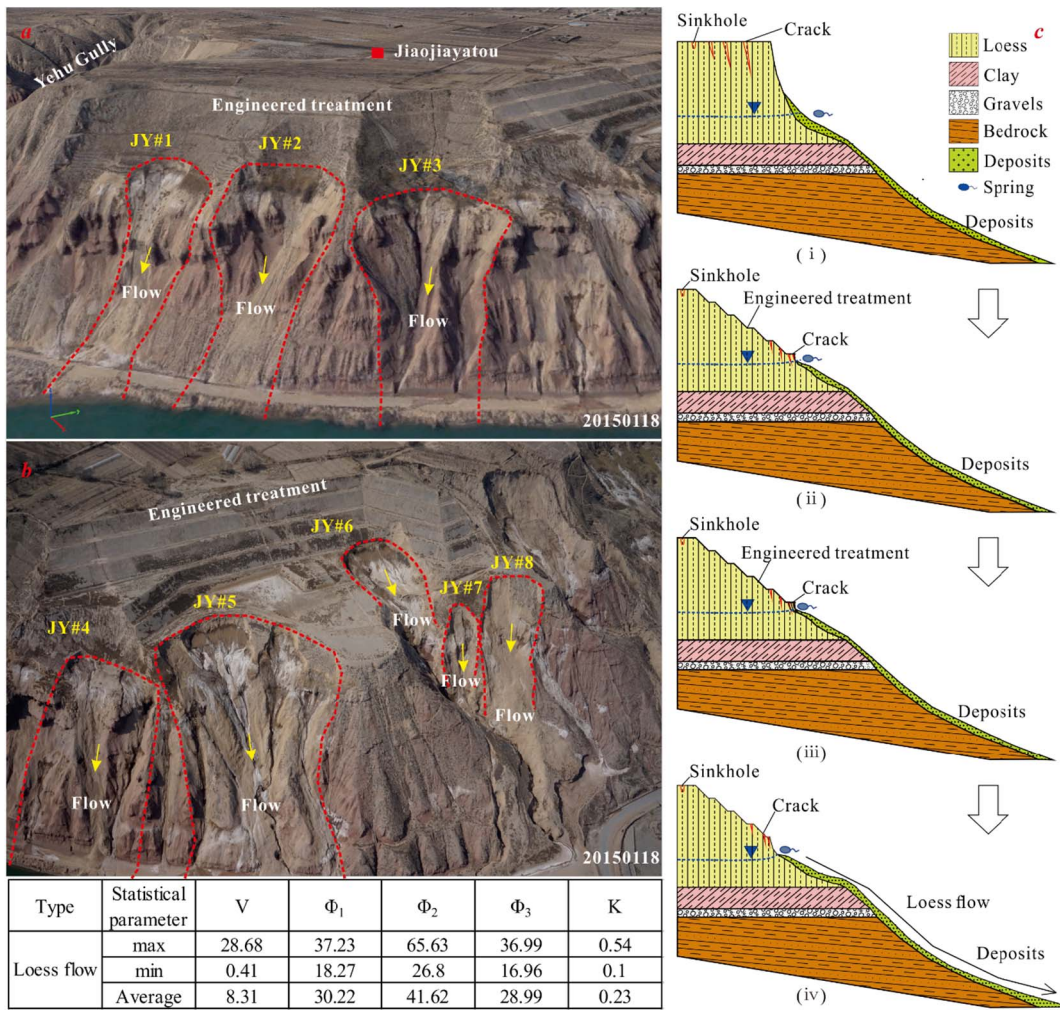
Fig. 10. Loess flows. (a) and (b) flows in S4; (c) Failure mode of loess flow; Geometric characteristics of flows are tabulated. Landslide locations see Fig. 1b.
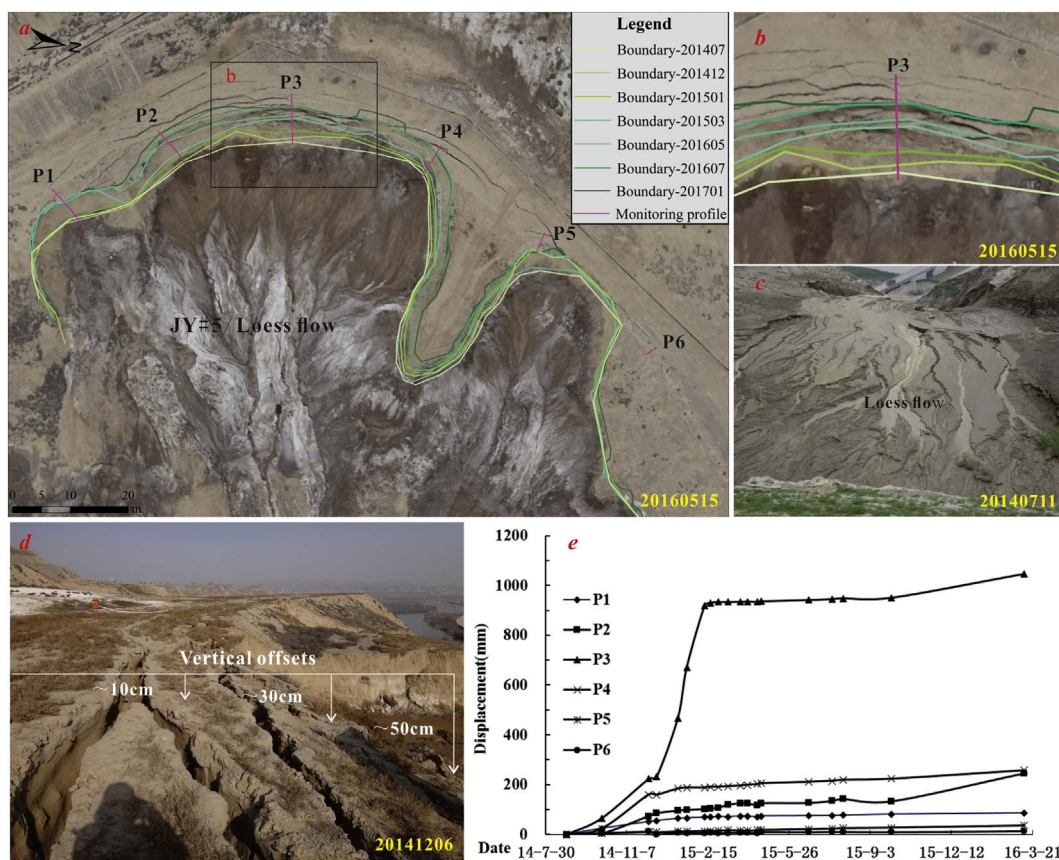
Fig. 11. JY#5 loess flow in S4 (location see Fig. 1b). (a) Boundaries of the most recent seven landslides (July 2014–Jan 2017), and cracks and monitoring profiles (image taken on May 5, 2016); (b) Enlarged monitoring profile P3; (c) A large amount of seepage and salt coating the bottom of the main scarp (photo taken on July 11, 2014); (d) Vertical offsets at the crown of loess flow varying 10–50 cm; (e) Field monitoring on the crack deformation by measure relative changes of surface markers (Aug 25, 2014–Mar 11, 2016).

Acknowledgements

References

Alimohammadlou, Y., Najafi, A., Yalcin, A., 2013. Landslide process and impacts: a proposed classification method. Catena 104, 219–232. http://dx.doi.org/10.1016/j.catena.2012.11.013.

Casagrande, A., 1940. Characteristics of cohesionless soils affecting the stability of slopes and earth fills. J. Boston Soc. Civ. Eng. 23, 257–276.

Cruden, D.M., Varnes, D.J., 1996. Landslide Types and Processes. Transportation research board, National Research Council Report Special Report. pp. 247.

Derbyshire, E., 2001. Geological hazards in loess terrain, with particular reference to the loess regions of China. Earth Sci. Rev. 54 (1–3), 231–260. http://dx.doi.org/10.1016/S0012-8252(01)00050-2.

Dijkstra, T.A., Rogers, C.D.F., Smalley, I.J., Derbyshire, E., Li, Y.J., Meng, X.M., 1994. The loess of north-central China: geotechnical properties and their relation to slope stability. Eng. Geol. 36, 153–171.

Ge, S.M., McKenzie, J., Voss, C., Wu, Q.B., 2011. Exchange of groundwater and surface-water mediated by permafrost response to seasonal and long term air temperature variation. Geophys. Res. Lett. 38 (14), L14402. http://dx.doi.org/10.1029/2011gl047911.

Görüm, T., Fan, X.M., van Westen, C.J., Huang, R.Q., Xu, Q., Tang, C., Wang, G.H., 2011. Distribution pattern of earthquake-induced landslides triggered by the 12 May 2008 Wenchuan earthquake. Geomorphology 133 (3–4), 152–167. http://dx.doi.org/10.1016/j.geomorph.2010.12.030.

Hungr, O., Evans, S.G., Bovis, M.J., Hutchinson, J.N., 2011. A review of the classification of landslides of the flow type. Environ. Eng. Geosci. 7 (3), 221–238.

Hungr, O., Leroueil, S., Picarelli, L., 2014. The Varnes classification of landslide types, an update. Landslides 11 (2), 167–194. http://dx.doi.org/10.1007/s10346-013-0436-y.

Hutchinson, J.N., 1988. General report: morphological and geotechnical parameters of landslides in relation to geology and hydrogeology. In: Proceedings of the 5th International Symposium on Landslides. Landslides, Lausanne, pp. 3–35.

Jiang, M.J., Zhang, F.G., Hu, H.J., Cui, Y.J., Peng, J.B., 2014. Structural characterization of natural loess and remolded loess under triaxial tests. Eng. Geol. 181, 249–260. http://dx.doi.org/10.1016/j.enggeo.2014.07.021.

Liu, Z., Liu, F.Y., Ma, F.L., Wang, M., Bai, X.H., Zheng, Y.L., Yin, H., Zhang, G.P., 2016. Collapsibility, composition, and microstructure of loess in China. Can. Geotech. J. 53 (4), 673–686. http://dx.doi.org/10.1139/cgj-2015-0285.

Lu, Z.Y., 1984. Basic charateristics of landslide distribution and main types landslides in China. In: International Symposium on Landslides, Toronto, pp. 411–418.

Meng, X.M., Derbyshire, E., 1998. Landslides and their control in the Chinese Loess Plateau models and case studies from Gansu Province, China. In: Maund, J.G., Eddleston, M. (Eds.), Geohazards in Engineering Geology. Geological Society. Engineering Geology Special Publications, Landon, 15, pp. 141–153.

Peng, D.L., Xu, Q., Qi, X., Fan, X.M., Dong, X.J., Li, S., Ju, Y.Z., 2016. Study on early recognition of loess landslides based on field investigation. Int. J. Geohazard. Environ. 2 (2), 35–52. http://dx.doi.org/10.15273/ijge.2016.02.006.

Qi, S.W., Xu, Q., Lan, H.X., Zhang, B., Liu, J.Y., 2010. Spatial distribution analysis of landslides triggered by 2008.5.12 Wenchuan Earthquake, China. Eng. Geol. 116 (1–2), 95–108. http://dx.doi.org/10.1016/j.enggeo.2010.07.011.

Qi, X., Xu, Q., Liu, F.Z., 2017. Analysis of retrogressive loess flowslides in Heifangtai, China. Eng. Geol. http://dx.doi.org/10.1016/j.enggeo.2017.08.028.

Smalley, I.J., Jefferson, I.F., Dijkstra, T.A., Derbyshire, E., 2001. Some major events in the development of the scientific study of loess. Earth Sci. Rev. 54 (1–3), 5–18. http://dx.doi.org/10.1016/S0012-8252(01)00038-1.

Varnes, D.J., 1978. Slope movement types and processes. In: Schuster, R.L., Krizek, R.J. (Eds.), Landslides: Analysis and control. vol. 176. Transportation Research Board Special Report, Washington, D.C., pp. 11–33 Special report.

Wang, Y.Z., Zhou, L.C., 1999. Spatial distribution and mechanism of geological hazards along the oil pipeline planned in western China. Eng. Geol. 51 (3), 195–201. http://dx.doi.org/10.1016/S0013-7952(98)00036-2.

Wei, L.J., 2012. Analysis of Cause and Sliding Distance on Loess Landslide in Heifangtai Area. Master. Lanzhou University.

Wu, W.J., Wang, N.Q., 2002. Basic types and active features of loess landslide. Chin. J. Geol. Harzard. Control 13 (2), 38–42 (in Chinese).

Wu, L.Z., Zhou, Y., Sun, P., Shi, J.S., Liu, G.G., Bai, L.Y., 2017. Laboratory character-ization of rainfall-induced loess slope failure. Catena 150, 1–8. http://dx.doi.org/10.1016/j.catena.2016.11.002.

Xu, L., Dai, F.C., Kwong, A.K.L., Min, H., 2008. Types and characteristics of loess land-slides at Heifangtai Loess Plateau, China. J. Mater. Sci Engl. 26 (3), 364–371 (in Chinese).

Xu, L., Dai, F.C., Tham, L.G., Tu, X.B., Jin, Y.L., 2011. Landslides in the transitional slopes between a Loess Platform and River Terrace, Northwest China. Environ. Eng. Geosci. 17 (3), 267–279.

Xu, L., Dai, F.C., Tu, X.B., Tham, L.G., Zhou, Y.F., Iqbal, J., 2014. Landslides in a loess platform, North-West China. Landslides 11 (6), 993–1005. http://dx.doi.org/10.1007/s10346-013-0445-x.

Xu, Q., Li, Y.R., Zhang, S., Dong, X.J., 2016. Classification of large-scale landslides in-duced by the 2008 Wenchuan earthquake, China. Environ. Earth Sci. 75 (1). http://dx.doi.org/10.1007/s12665-015-4773-0.

Yuan, Z.X., Wang, L.M., 2009. Collapsibility and seismic settlement of loess. Eng. Geol. 105 (1–2), 119–123. http://dx.doi.org/10.1016/j.enggeo.2008.12.002.

Zeng, R.Q., Meng, X.M., Zhang, F.Y., Wang, S.Y., Cui, Z.J., Zhang, M.S., Zhang, Y., Chen, G., 2016. Characterizing hydrological processes on loess slopes using electrical re-sistivity tomography – a case study of the Heifangtai Terrace, Northwest China. J. Hydrol. 541, 742–753. http://dx.doi.org/10.1016/j.jhydrol.2016.07.033.

Zhang, F.Y., Wang, G.H., Kamai, T., Chen, W.W., Zhang, D.X., Yang, J., 2013. Undrained shear behavior of loess saturated with different concentrations of sodium chloride solution. Eng. Geol. 155, 69–79. http://dx.doi.org/10.1016/j.enggeo.2012.12.018.

Zhou, J.X., Zhu, C.Y., Zheng, J.M., Wang, X.H., Liu, Z.H., 2002. Landslide disaster in the loess area of China. J. For. Res. 13 (2), 157–161.

Zhou, Y.F., Tham, L.G., Yan, W.M., Dai, F.C., Xu, L., 2014. Laboratory study on soil be-havior in loess slope subjected to infiltration. Eng. Geol. 183, 31–38. http://dx.doi.org/10.1016/j.enggeo.2014.09.010.